Hybrid Open-Framework Iron Phosphate – Oxalates Demonstrating a Dual Role of the Oxalate Unit

Amitava Choudhury,[a, b] Srinivasan Natarajan,[a] and C.N.R. Rao*[a, b]

Abstract: New inorganic – organic hybrid open-framework materials of the phosphate – oxalate family, $[Fe_2(H_2O)_2(HPO_4)_2(C_2O_4)]\cdot H_2O$ (**I**), $[Fe_2(H_2O)_2(HPO_4)_2(C_2O_4)]\cdot 2H_2O$ (**II**), $[C_3N_2H_{12}][Fe_2(HPO_4)_2(C_2O_4)_{1.5}]_2$ (**III**), and $[C_3N_2OH_{12}][Fe_2(HPO_4)_2(C_2O_4)_{1.5}]_2$ (**IV**) have been synthesized hydrothermally in the presence of structure-directing amines. The amine molecules are incorporated in **III** and **IV**, whereas **I** and **II** are devoid of them. The oxalate units act as a bridge between the layers in all the compounds. The layers in **I** and **II** are entirely inorganic, being formed by FeO_6 and PO_4 units, whereas in **III** and **IV** oxalate units constitute the inorganic layers and act as the bridge between these layers. Such a dual role of the oxalate unit is unique and noteworthy. The formation of two types of inorganic layers in **I** and **II** consisting of four-, six-, and eight-membered rings, indicates the interconversions between the various rings in the phosphate – oxalates to be facile. All the phosphate – oxalates show antiferromagnetic ordering at low temperatures.

Keywords: bridging ligands · crystal growth · iron · phosphorus · X-ray scattering

Introduction

Of the various inorganic open-framework materials discovered in the last few years, the metal phosphates occupy a prime position. The family of open-framework metal phosphates includes one-dimensional chains or ladders, two-dimensional layers, and three-dimensional structures.[1] An interesting variant of the metal phosphate is that obtained by incorporating the oxalate unit in the materials.[2] A few metal phosphate – oxalates, especially those of iron, constituting a novel kind of inorganic – organic hybrid materials, have been reported during the last year.[3–7] The important structural features of these compounds is the presence of iron phosphate sheets, crosslinked by the oxalate units giving rise to the three-dimensional architecture. We have been investigating phosphate – oxalates not only with a view to producing new materials but also to unravelling the structural features of these novel hybrid material, and we have succeeded in isolating iron phosphate – oxalates with a variety of structural features. Two of the iron phosphate – oxalates discovered by us possess iron phosphate layers that are crosslinked by oxalate bridges. The layers in these materials consist of different ring systems reminiscent of the open-framework metal phosphates. More importantly, we have obtained iron phosphate – oxalates wherein the oxalate unit, besides acting as a bridge between the metal phosphate layers, is part of the layer system. The presence of oxalates performing two functions in these hybrid materials is noteworthy. Such a dual role of the oxalate unit has also been found by us in a metal oxalate structure. Thus, the oxalate unit in iron phosphate – oxalates acts like the phosphate unit in metal phosphates and as the oxalate unit in metal oxalates.

[a] Prof. Dr. C.N.R. Rao, A. Choudhury, Dr. S. Natarajan
Chemistry and Physics of Materials Unit and
CSIR Centre of Excellence in Chemistry
Jawaharlal Nehru Centre for Advanced Scientific Research
Jakkur P.O., Bangalore 560 064 (India)
Fax: (+91) 80-846-2766
E-mail: cnrrao@jncasr.ac.in

[b] Prof. Dr. C.N.R. Rao, A. Choudhury
Solid State and Structural Chemistry Unit
Indian Institute of Science, Bangalore 560 012 (India)

Results and Discussion

$[Fe_2(H_2O)_2(HPO_4)_2(C_2O_4)]\cdot H_2O$ (I) and $[Fe_2(H_2O)_2(HPO_4)_2(C_2O_4)]\cdot 2H_2O$ (II): The asymmetric units of **I** and **II** are identical and each consist of 11 non-hydrogen atoms (Figure 1). Both **I** and **II**, have three-dimensional structures built from a networking of FeO_6 octahedra, PO_4 tetrahedra, and oxalate units. The FeO_6 octahedra and PO_4 tetrahedra form layers that are held together and apart by the cross-linking oxalate groups. Of the six oxygen atoms of a Fe octahedron, three belong to the phosphate groups and two to the oxalate units, while the remaining oxygen atom is a terminal water molecule.

In **I**, the FeO_6 octahedra and PO_4 tetrahedra strictly alternate along the *b* axis forming a layer possessing six-membered apertures (made up of 6 T atoms, T = Fe, P, Figure 2). Layers exclusively possessing six-membered aper-

0947-6539/00/0607-1168 $ 17.50+.50/0 *Chem. Eur. J.* **2000**, *6*, No. 7

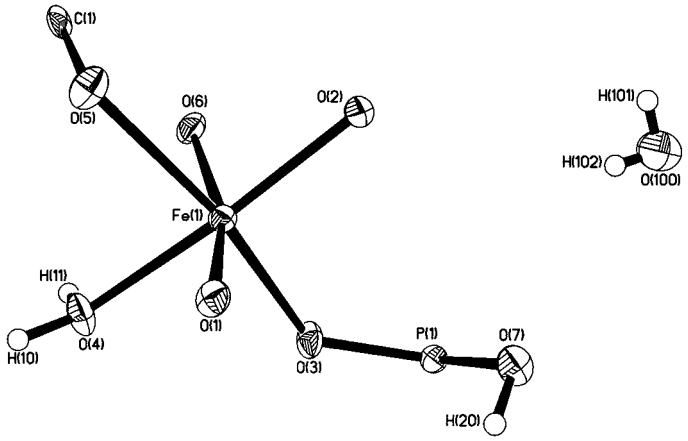

Figure 1. ORTEP plot of the asymmetric unit in **I** and **II**. Thermal ellipsoids are given at 50% probability.

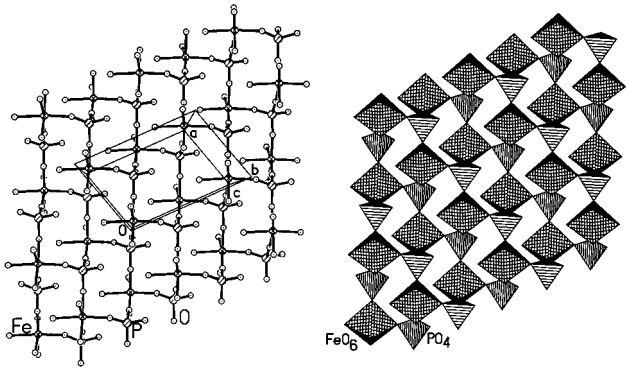

Figure 2. Structure of **I** showing the layers made by the networking of FeO_6 and PO_4 units. Note that the layers are made of six-membered rings. Left: Ball-and-stick view; right: polyhedral view.

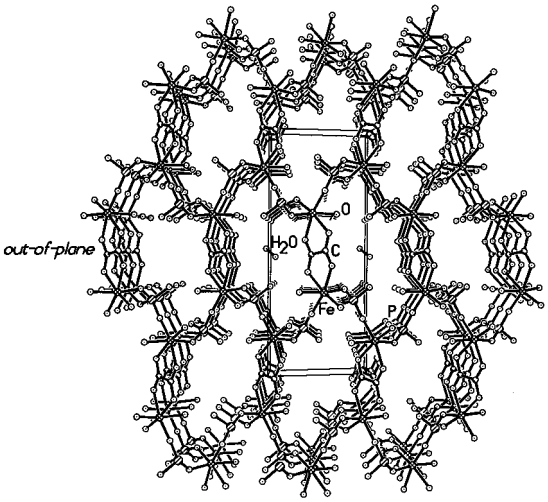

Figure 3. Structure of **I** showing the channels. The *out-of-plane* oxalate unit bridges the layers, and the water molecules are present in the channels. Hydrogen atoms are omitted for clarity.

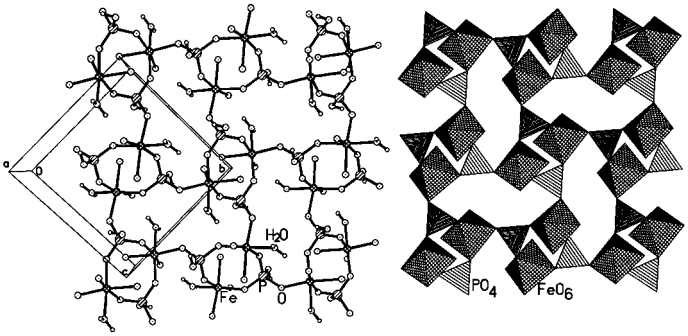

Figure 4. Structure of **II** along the *bc* plane showing the layers. The layers are made by four- and eight-membered rings, and the bound water molecule from the Fe center protrude into the eight-membered aperture. Left: Ball-and-stick view; right: polyhedral view.

tures are rare, the only other example being a tin(II) phosphate–oxalate.[2] The layers are connected through the anionic oxalate bridges (*out-of-plane* oxalate units) completing the neutral three-dimensional architecture. Along the *a* axis, the connectivity produces eight-membered one-dimensional channels wherein the bonded water and the free water molecules reside (Figure 3).

In **II**, the strictly alternating FeO_6 and PO_4 moieties form four- and eight-membered apertures (made up of 4 and 8 T atoms, respectively) along the *bc* plane (Figure 4). The water molecules attached to the iron centers project into the eight-membered apertures. The oxalate units link these layers completing the three-dimensional connectivity. Along the *a* axis, the eight-membered apertures form one-dimensional channels (Figure 5).

Selected bond lengths and angles of **I** and **II** are given in Tables 1 and 2 respectively. The three different types of Fe–O bonds (Fe–O–P; Fe–O–C; $Fe–O_{Water}$) show the expected differences in average bond lengths and angles. The phosphorus atoms are connected to three neighboring iron atoms through the oxygens, and have a terminal OH group. Bond valence sum calculations[8] indicate that one of the oxygen atoms [O(4)] is a water molecule and that the one bound to P [O(7)] is a terminal hydroxy group. The bonding of water molecules directly to the iron center is not uncommon, and similar bonding is known in open-framework iron phosphate materials.[9] The observed bond lengths and angles observed in **I** and **II** are in general agreement with those reported in the literature.

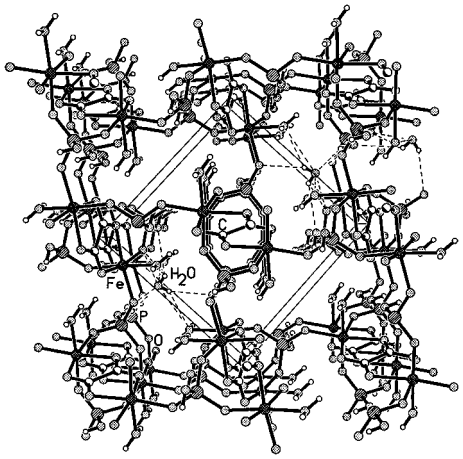

Figure 5. Structure of **II** along *a* axis, showing channels.

Table 1. Selected bond lengths [Å] and angles [°] for **I**.

Fe(1)–O(1)	1.893(3)	Fe(1)–O(2)	1.936(3)
Fe(1)–O(3)	1.948(2)	Fe(1)–O(4)	2.082(3)
Fe(1)–O(5)	2.102(2)	Fe(1)–O(6)	2.125(2)
P(1)–O(1)$^{\#1}$	1.508(3)	P(1)–O(2)	1.517(3)
P(1)–O(3)$^{\#2}$	1.528(2)	P(1)–O(7)	1.564(3)
C(1)–O(5)	1.249(4)	C(1)$^{\#3}$–O(6)	1.255(4)
C(1)–C(1)$^{\#3}$	1.536(6)		
O(3)-Fe(1)-O(4)	93.55(11)	O(1)-Fe(1)-O(5)	167.86(10)
O(2)-Fe(1)-O(5)	90.43(10)	O(3)-Fe(1)-O(5)	90.47(10)
O(4)-Fe(1)-O(5)	85.16(13)	O(1)-Fe(1)-O(6)	92.27(11)
O(2)-Fe(1)-O(6)	86.58(10)	O(3)-Fe(1)-O(6)	168.20(9)
O(4)-Fe(1)-O(6)	84.39(11)	O(5)-Fe(1)-O(6)	77.79(9)
O(1)$^{\#1}$-P(1)-O(2)	111.9(2)	O(1)$^{\#1}$-P(1)-O(3)$^{\#2}$	109.10(14)
O(2)-P(1)-O(3)$^{\#2}$	113.08(14)	O(1)$^{\#1}$-P(1)-O(7)	108.7(2)
O(1)-Fe(1)-O(2)	95.98(11)	O(2)-P(1)-O(7)	107.7(2)
O(1)-Fe(1)-O(3)	99.24(11)	O(1)$^{\#2}$-P(1)-O(7)	106.10(14)
O(2)-Fe(1)-O(3)	94.77(11)	O(5)-C(1)-O(6)$^{\#3}$	127.0(3)
O(1)-Fe(1)-O(4)	86.96(13)	O(5)-C(1)-C(1)$^{\#3}$	116.9(4)
O(2)-Fe(1)-O(4)	170.62(12)	O(6)$^{\#3}$-C(1)-C(1)$^{\#3}$	116.1(4)

Symmetry transformations used to generate equivalent atoms: #1: $x, -y+3/2, z+1/2$; #2: $x-1, y, z$; #3: $-x, -y+1, -z+1$.

Table 2. Selected bond lengths [Å] and angles [°] for **II**.

Fe(1)–O(1)	1.935(3)	Fe(1)–O(2)	1.935(3)
Fe(1)–O(3)	1.942(3)	Fe(1)–O(4)	2.088(4)
Fe(1)–O(5)	2.104(3)	Fe(1)–O(6)	2.110(3)
P(1)–O(2)$^{\#1}$	1.521(3)	P(1)–O(1)$^{\#2}$	1.527(3)
P(1)–O(3)	1.530(3)	P(1)–O(7)	1.578(3)
C(1)–O(5)	1.244(5)	C(1)–O(6)$^{\#3}$	1.259(5)
C(1)–C(1)$^{\#3}$	1.535(8)		
O(3)-Fe(1)-O(4)	83.03(13)	O(1)-Fe(1)-O(5)	87.69(12)
O(2)-Fe(1)-O(5)	94.42(13)	O(3)-Fe(1)-O(5)	167.84(13)
O(4)-Fe(1)-O(5)	85.52(13)	O(1)-Fe(1)-O(6)	164.92(12)
O(2)-Fe(1)-O(6)	88.43(12)	O(3)-Fe(1)-O(6)	96.02(12)
O(4)-Fe(1)-O(6)	81.0(2)	O(5)-Fe(1)-O(6)	78.10(12)
O(2)$^{\#1}$-P(1)-O(1)$^{\#2}$	112.5(2)	O(2)$^{\#1}$-P(1)-O(3)	110.4(2)
O(1)$^{\#2}$-P(1)-O(3)	111.7(2)	O(2)$^{\#1}$-P(1)-O(7)	109.1(2)
O(1)-Fe(1)-O(2)	97.78(13)	O(1)$^{\#2}$-P(1)-O(7)	104.0(2)
O(1)-Fe(1)-O(3)	96.96(13)	O(3)-P(1)-O(7)	108.8(2)
O(2)-Fe(1)-O(3)	96.07(12)	O(5)-C(1)-O(6)$^{\#3}$	126.9(4)
O(1)-Fe(1)-O(4)	93.0(2)	O(5)-C(1)-C(1)$^{\#3}$	116.9(5)
O(2)-Fe(1)-O(4)	169.2(2)	O(6)$^{\#3}$-C(1)-C(1)$^{\#3}$	116.3(5)

Symmetry transformations used to generate equivalent atoms: #1: $-x+1, y+1/2, -z+3/2$; #2: $x, -y+1/2, z-1/2$; #3: $-x+2, -y, -z+2$.

$[C_3N_2H_{12}][Fe_2(HPO_4)_2(C_2O_4)_{1.5}]_2$ (III) and $[C_3N_2OH_{12}][Fe_2(HPO_4)_2(C_2O_4)_{1.5}]_2$ (IV): The asymmetric units of **III** and **IV** contain 24 and 25 non-hydrogen atoms, respectively, with two crystallographically distinct iron and phosphorus atoms (Figure 6). The final atomic coordinates for **III** are presented in Table 3. The structure consists of layers of formula $[Fe_2(HPO_4)_2(C_2O_4)]$, linked through another oxalate unit to complete the anionic framework. Charge neutrality is achieved by the incorporation of organic amines in their diprotonated form. Thus, there are $0.5\,[C_3N_2H_{12}]^{2+}$ molecules in **III** and $0.5\,[C_3N_2OH_{12}]^{2+}$ molecules in **IV**, respectively, per framework formula. The structure comprises a network of FeO_6, PO_4, and C_2O_4 moieties with each iron bound to six oxygens, which are, in turn bound to carbon and phosphorus atoms completing the network.

The structures of **III** and **IV** are made from a networking of FeO_6, PO_4, and C_2O_4 forming layers. Of the two iron atoms in the asymmetric unit, Fe(1) is connected to two oxalate and

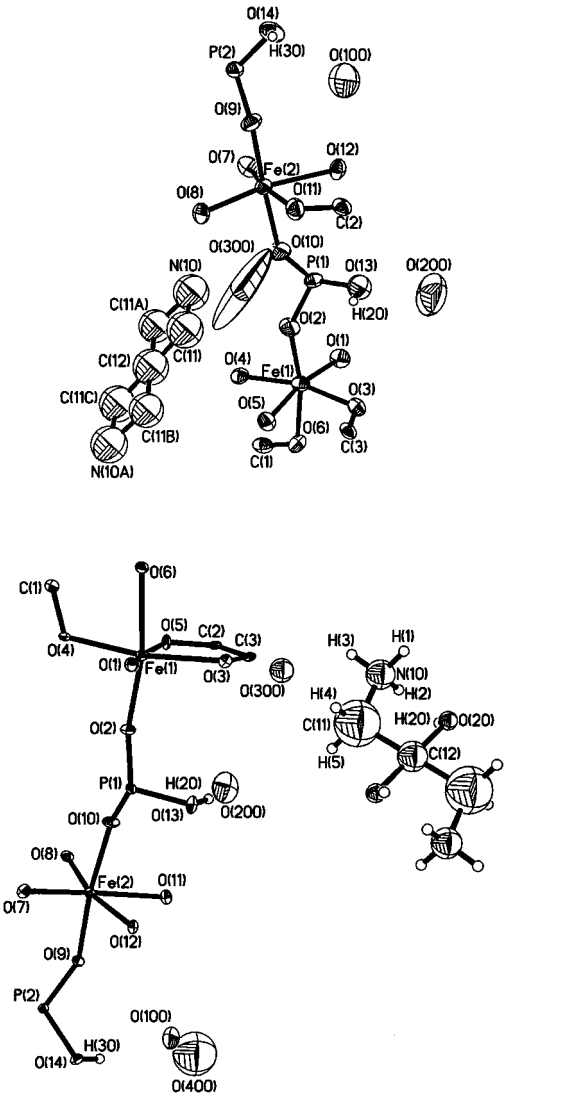

Figure 6. Top: ORTEP plot of **III**. Thermal ellipsoids are given at 50% probability. Bottom: ORTEP plot of **IV**. Thermal ellipsoids are given at 50% probability.

phosphate units, and Fe(2) is bonded with one oxalate and four phosphate units. The FeO_6 and PO_4 units are connected to each other in such a way that they form zigzag one-dimensional ladderlike chains that are linked through an oxalate unit to form an oxalate–phosphate layer (Figure 7). This is indeed a unique inorganic–organic hybrid layer network. The hybrid layers are linked through another oxalate unit acting like a bridge (Figure 8). Thus, two different types of oxalate units occur in **III** and **IV**. One *in-plane* (with respect to the layer) and the other *out-of-plane*. To our knowledge, this is the first example of the existence of two different types of oxalate moieties in such a material.

The linkages between the oxalates and the oxalate–phosphate layers in **III** and **IV** create channels of width 5.2×4.5 Å (shortest atom–atom contact distance not including the van der Waals radii) along *a* axis (Figure 8). Figure 9 shows the connectivity along the *c* axis. Thus, **III** and **IV** are members of three-dimensional solids possessing different channels. All the iron atoms are hexacoordinated with respect to oxygen. Of the two crystallographically independent iron atoms in **III**

0947-6539/00/0607-1170 $ 17.50+.50/0 *Chem. Eur. J.* **2000**, *6*, No. 7

Table 3. Atomic coordinates [$\times 10^4$] and equivalent isotropic displacement parameters [$Å^2 \times 10^3$] for **III**.

Atom	*x*	*y*	*z*	*U*(eq)[a]
Fe(1)	6348(1)	1125(1)	6645(1)	24(1)
Fe(2)	12478(1)	619(1)	10020(1)	22(1)
P(1)	8945(2)	1073(2)	8908(2)	24(1)
P(2)	15512(2)	– 30(2)	11833(2)	23(1)
O(1)	5195(7)	829(4)	7747(5)	33(2)
O(2)	8243(6)	1005(4)	7643(5)	34(2)
O(3)	6001(7)	2432(4)	6906(5)	30(2)
O(4)	6675(6)	– 74(4)	5978(5)	28(2)
O(5)	7383(6)	1693(4)	5436(5)	28(2)
O(6)	4444(1)	1046(4)	5347(5)	29(2)
O(7)	11847(7)	– 521(4)	10366(5)	35(2)
O(8)	13183(6)	318(4)	8670(5)	35(2)
O(9)	14422(6)	532(4)	11019(5)	30(2)
O(10)	10540(6)	849(4)	8996(5)	40(2)
O(11)	12936(7)	1969(4)	9834(5)	31(2)
O(12)	11571(6)	1214(4)	11337(5)	26(2)
O(13)	8828(8)	2041(4)	9319(6)	51(2)
O(14)	16170(7)	540(4)	12900(5)	39(2)
C(1)	4352(10)	324(6)	4817(8)	29(2)
C(2)	12386(9)	2480(6)	10448(7)	25(2)
C(3)	6578(9)	2957(6)	6311(7)	24(2)
O(100)	15052(13)	2098(6)	12736(8)	114(4)
O(200)	6432(11)	2231(8)	10239(10)	128(4)
O(300)	13122(42)	2458(24)	7633(26)	738(42)
N(10)[b]	10318(15)	– 363(9)	7045(11)	109(4)
C(12)[b]	10000	0	5000	107(8)
C(11A)[b]	9926(33)	– 744(10)	5874(12)	95(14)
C(11)[b]	10521(35)	352(13)	6199(9)	110(15)

[a] *U*(eq) is defined as one third of the trace of the orthogonalized U_{ij} tensor. [b] Refined isotropically.

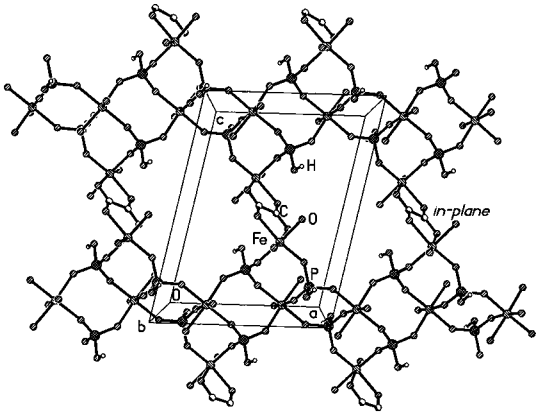

Figure 7. Structure of **III** along the *a* axis, showing the ladder like chains and the connecting oxalate unit (*in-plane* oxalate) forming a hybrid layer.

and **IV**, Fe(1) is coordinated with four oxygen atoms with distances in the range 2.041 – 2.101 Å (av 2.068 Å, for **III**, 2.074 Å for **IV**) and two oxygen atoms have distances in the range 1.893 – 1.916 Å (av 1.915 Å for **III**, 1.90 Å for **IV**). Fe(2), on the other hand, is coordinated with two oxygen atoms in the range 2.116 – 2.148 Å (av 2.128 Å for **III**, 2.133 Å for **IV**) and four oxygen atoms in the range 1.902 – 1.981 Å (av 1.939 Å for **III**, 1.946 Å for **IV**). These are the oxygen atoms linked to phosphorus and carbon atoms, respectively. Similar bond lengths have been observed before. The O-Fe-O bond angles are as expected. The P–O and C–O distances and O-P-O and O-C-O bond angles are in the range expected for this

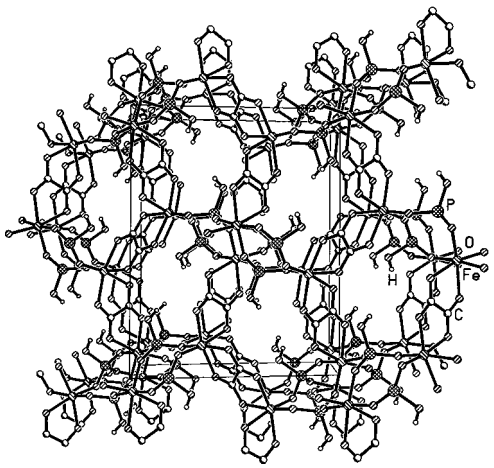

Figure 8. Structure of **III** showing channels along the *a* axis formed by the bridging oxalates with the hybrid layer.

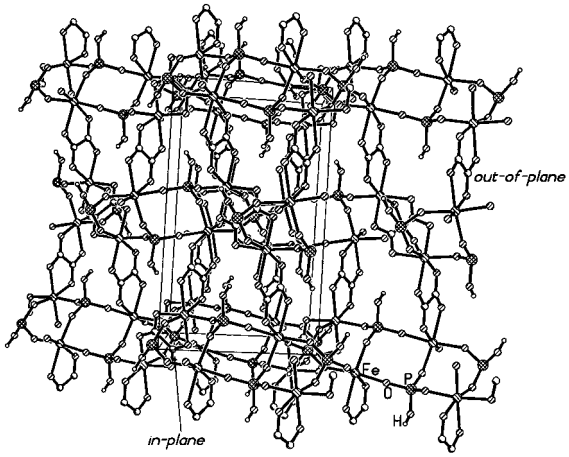

Figure 9. Structure of **III** showing channels along the *c* axis. Note the two different types of oxalate units (*in-plane* and *out-of-plane*).

type of bonding. Similar structural parameters have been observed for other phosphate-oxalates. Bond valence sum calculations[8] indicate that two of the oxygen atoms attached to the phosphorus atom have a hydrogen atom attached to it making it a terminal OH group. The selected bond lengths and angles for **III** are presented in Table 4. We have not given the various structural details of **IV** since they are very similar to those of **III**.

The iron phosphate – oxalates **I** – **IV** are members of a new family of inorganic – organic hybrid framework structures and have been obtained as good quality single crystals by employing hydrothermal methods. Although all these materials involve bonding between the iron atoms and the phosphate, oxalate units, they exhibit interesting differences. While **III** and **IV** are formed with the amine in the final framework solid, **I** and **II** are formed devoid of them. Such elimination of amines during the hydrothermal synthesis is known.[2, 10] It is noteworthy that although **I** and **II** are formed under identical conditions of composition and temperature with only a slight difference in the duration of reaction, the resultant products possess perceptible differences in structural features. In the few known iron phosphate – oxalates, the iron phosphate layers are neutral and the anionicity of the framework is

Table 4. Selected bond lengths [Å] and angles [°] in **III**.

Fe(1)−O(1)	1.916(6)	Fe(2)−O(7)	1.902(6)
Fe(1)−O(2)	1.914(6)	Fe(2)−O(8)	1.927(6)
Fe(1)−O(3)	2.046(6)	Fe(2)−O(9)	1.945(6)
Fe(1)−O(4)	2.041(6)	Fe(2)−O(10)	1.981(6)
Fe(1)−O(5)	2.085(6)	Fe(2)−O(11)	2.116(6)
Fe(1)−O(6)	2.101(6)	Fe(2)−O(12)	2.140(6)
P(1)−O(10)	1.491(6)	P(2)−O(9)	1.514(6)
P(1)−O(2)	1.531(6)	P(2)−O(1)$^{\#1}$	1.514(6)
P(1)−O(7)$^{\#1}$	1.505(9)	P(2)−O(8)$^{\#2}$	1.519(6)
P(1)−O(13)	1.562(7)	P(2)−O(14)	1.565(6)
C(1)−O(4)$^{\#3}$	1.259(10)	C(2)−O(5)$^{\#5}$	1.256(10)
C(3)−O(12)$^{\#4}$	1.260(10)	C(1)−C(1)$^{\#3}$	1.54(2)
C(2)−C(3)$^{\#5}$	1.548(12)	N(10)−C(11)	1.528(10)
N(10)−C(11A)	1.499(10)	C(11)−C(12)	1.522(10)
C(11A)−C(12)	1.556(10)		
O(2)-Fe(1)-O(1)	96.1(3)	O(7)-Fe(2)-O(8)	98.0(3)
O(2)-Fe(1)-O(4)	88.4(2)	O(7)-Fe(2)-O(9)	94.9(3)
O(1)-Fe(1)-O(4)	102.2(2)	O(8)-Fe(2)-O(9)	94.5(2)
O(2)-Fe(1)-O(3)	98.5(3)	O(7)-Fe(2)-O(10)	91.2(3)
O(1)-Fe(1)-O(3)	89.7(3)	O(8)-Fe(2)-O(10)	86.2(3)
O(4)-Fe(1)-O(3)	165.6(2)	O(9)-Fe(2)-O(10)	173.7(3)
O(2)-Fe(1)-O(5)	89.4(2)	O(7)-Fe(2)-O(11)	169.7(2)
O(1)-Fe(1)-O(5)	168.3(2)	O(8)-Fe(2)-O(11)	91.8(3)
O(4)-Fe(1)-O(5)	88.2(2)	O(9)-Fe(2)-O(11)	87.3(2)
O(3)-Fe(1)-O(5)	79.3(2)	O(10)-Fe(2)-O(11)	86.4(3)
O(2)-Fe(1)-O(6)	167.6(2)	O(7)-Fe(2)-O(12)	92.2(2)
O(1)-Fe(1)-O(6)	90.2(3)	O(8)-Fe(2)-O(12)	167.8(2)
O(4)-Fe(1)-O(6)	79.9(2)	O(9)-Fe(2)-O(12)	91.2(2)
O(3)-Fe(1)-O(6)	92.1(2)	O(10)-Fe(2)-O(12)	87.0(2)
O(5)-F1(1)-O(6)	86.4(2)	O(11)-Fe(2)-O(12)	77.7(2)
O(10)-P(1)-O(7)$^{\#1}$	114.8(4)	O(10)-P(1)-O(2)	105.3(4)
O(7)$^{\#1}$-P(1)-O(2)	112.6(4)	O(10)-P(1)-O(13)	108.9(4)
O(7)$^{\#1}$-P(1)-O(13)	105.5(4)	O(2)-P(1)-O(13)	109.7(4)
O(9)-P(2)-O(1)$^{\#1}$	113.3(3)	O(9)-P(2)-O(8)$^{\#2}$	112.2(3)
O(1)$^{\#1}$-P(2)-O(8)$^{\#2}$	109.4(4)	O(9)-P(2)-O(14)	108.2(3)
O(1)$^{\#1}$-P(2)-O(14)	106.9(3)	O(8)$^{\#2}$-P(2)-O(14)	106.4(4)
O(4)$^{\#3}$-C(1)-O(6)	127.4(8)	O(11)-C(2)-O(5)$^{\#5}$	128.0(8)
O(12)$^{\#4}$-C(3)-O(3)	127.8(8)	N(10)-C(11A)-C(12)	108.7(11)
N(10)-C(11)-C(12)	109.0(11)	C(11)$^{\#6}$-C(12)-C(11)	109.7(10)

Symmetry transformations used to generate equivalent atoms: #1: $-x+2$, $-y$, $-z+2$; #2: $-x+3$, $-y$, $-z+2$; #3: $-x+1$, $-y$, $-z+1$; #4: $x+1/2$, $-y+1/2$, $z-1/2$; #5: $x+1/2$, $-y+1/2$, $z+1/2$; #6: $-x+2$, $-y$, $-z+1$.

derived from the oxalate bridges. In **I** and **II**, however, cationic iron phosphate layers are neutralized by the oxalate bridges to render the framework neutral.

The amine molecules in **III** and **IV** (1,3-diaminopropane (1,3-DAP) and 1,3-diamino-2-hydroxy propane (1,3-DAHP), respectively) are disordered along with the water molecules within the channels. The disorder in the case of 1,3-DAP occurs on the carbon atom attached to the nitrogen atom and in 1,3-DAHP, it is the oxygen atom on the central carbon atom that is disordered. Disorder of the amine molecules in open-framework solids is not uncommon, and most of the earlier observations relate to the terminal atoms[11] and only recently disorder of the amine molecules involving nonterminal atoms has been observed.[12]

The coordination environment and connectivity of Fe atoms in **I**–**IV** presents an interesting comparison. Though all the Fe atoms are octahedrally coordinated, the manner they link up with the phosphate and oxalates units show distinct differences. In **I** and **II** the iron atoms do not show any differences and in **III** and **IV** the iron atoms presents two different coordination environments. In **III** and **IV**, Fe(1) is bonded to two oxalate and two phosphate units, and Fe(2) is bonded to one oxalate and four phosphate units. This is possibly due to the ambidendate coordinating ability of the oxalate units requiring two phosphate units to make similar connections as that of one oxalate unit.

The framework composition of **I** and **II** is similar, but there are differences in the networking of the polyhedra. Compound **I** forms layers made up of six-membered apertures within the layers, **II** possess four- and eight-membered apertures. It is proposed that the four-memberd rings can readily transform to six-, eight-, and other higher membered rings.[13] In the case of **I** and **II**, ring conversions could occur as shown in Scheme 1. The six-membered ring within the layers

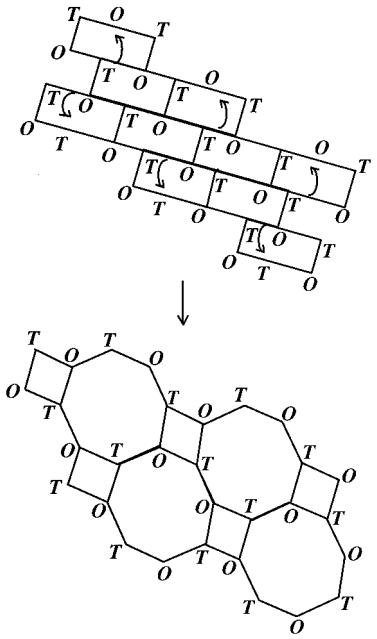

Scheme 1. Schematic representation of a possible conversion between the six-membered ring aperture of **I** into four- and eight-membered apertures in **II**. Note that oxygen atoms are not shown and only bond shifting is indicated. O and T represent octahedral (Fe) and tetrahedral (P) atoms respectively.

of **I** can readily transformed to four- and eight-membered rings of **II** by a simple shifting of bonds. In general, *n*-edge-sharing four-membered rings can give rise to a ring with $4n-2(n-1)$ atoms. Or, if we add *n* four-membered rings to a *m*-membered ring, we get a ring with $m+2n$ atoms (*m* and *n* represent T atoms; T = Fe, P in the present case). The facile transformations of these ring structures within the layers of **I** and **II** suggests that one is dealing with structures of comparable energies that render it difficult to exactly pin-down the stepwise mechanism involved in these transformations.

The layers in **III** and **IV** are different from those in **I** and **II**. Whereas the layers in **I** and **II** are formed by the linkages between the FeO_6 octahedra and PO_4 tetrahedra, the layers in **III** and **IV** are made by linkages involving the (*in-plane*) C_2O_4 units, in addition to the FeO_6 and PO_4. The layers are crosslinked by the (*out-of-plane*) oxalate units in all the phosphate–oxalates. Such a dual role of the oxalate unit has

0947-6539/00/0607-1172 $ 17.50+.50/0 *Chem. Eur. J.* **2000**, *6*, No. 7

not been observed previously. Significantly, we have just discovered a zinc oxalate containing both the *in-plane* and *out-of-plane* oxalate linkages with three-dimensional connectivity.[14] In Figure 10, we show the structure of this material to illustrate the presence of the oxalates within the layers as well as a bridge between the layers. This dual functionality of the oxalate units, in the Zn oxalate, gives rise to an elliptical aperture made by the linkages between 10 Zn and 10 oxalate units within the same plane, with the other oxalate unit connecting the elliptical pores such that two such rings are perpendicular to each other (Figure 10 bottom).

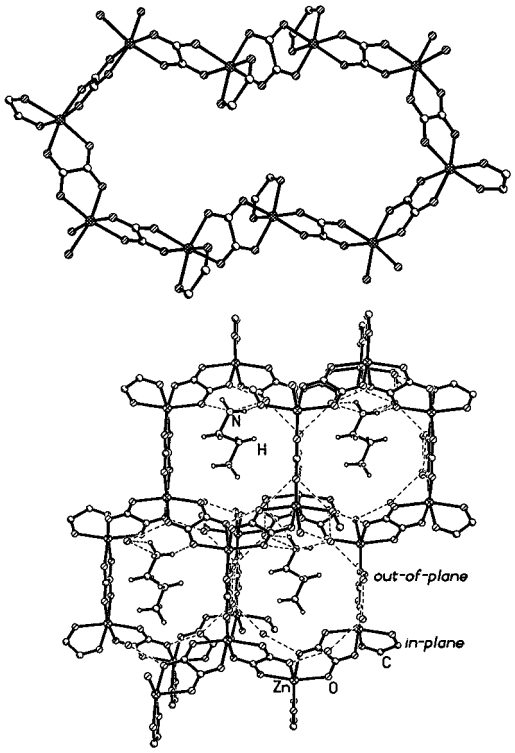

Figure 10. Top: Structure showing the two types of oxalate units in a zinc oxalate. Note that one of zinc atoms is coordinated to two oxalate units going out of plane leading to three-dimensional connectivity. Bottom: Three-dimensional zinc oxalate structure showing the channels formed by the oxalate units. Note the presence of two types of oxalate units (*in-plane* and *out-of-plane*).

The coordination environment of iron atoms in phosphates and oxalates also presents an interesting comparison. While in most of the phosphate-based open-framework structures iron is essentially either five- or six-coordinate, forming a trigonal bipyramidal FeO_5 or octahedral FeO_6 as the building units, in oxalates[15] and phosphate – oxalates[4–7] including the present solids, iron is present exclusively in an octahedral environment. We believe that this is because the average charge per oxygen atom on the oxalate (0.5) is less than that on the phosphate (0.75), so that more oxalate oxygen atoms are needed to satisfy the valence of iron.

Magnetic susceptibility measurements indicate strong antiferromagnetic interactions in **I**–**IV**, with the Neel temperature in the range 25–40 K (Figure 11). The magnetic behavior above the ordering temperature obeys Curie–Weiss behavior. The various magnetic parameters are given in Table 5. The μ_{eff} calculated from the Curie–Weiss law

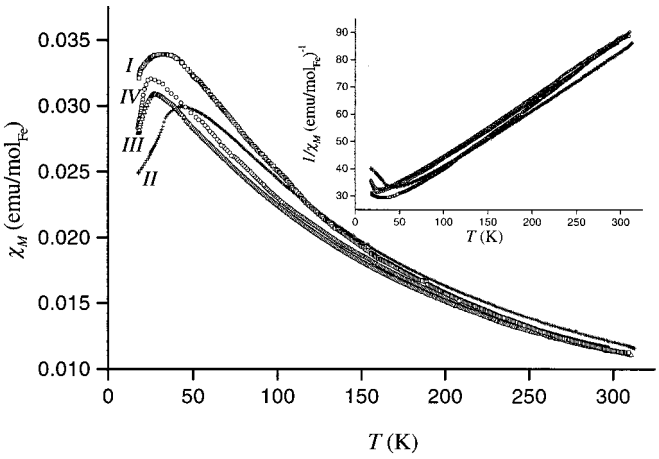

Figure 11. Temperature dependence of magnetic susceptibility for compounds **I**–**IV**. Inset shows inverse of the susceptibility.

Table 5. Magnetic parameters for compounds **I**–**IV**.

Compound	θp	T_N [K]	μ_{eff}
I	– 63.1	30	5.73
II	– 90.9	40	6.15
III	– 88.8	25	6.13
IV	– 92.3	25	6.01

shows that iron is present in the high-spin state in all the compounds.

Thermogravimetric analysis (TGA) of **I**–**IV** was carried out in flowing nitrogen in the range 30–700 °C. Compounds **I** and **II** showed three steps of decomposition. The first mass loss occurring at 150 °C (4% for **I** and 8.3% for **II**) corresponds to the loss of free water molecule (calcd 4.04% for **I** and 7.8% for **II**), the second mass loss of about 23% in the range 220–290 °C corresponds to the loss of bound water and oxalate molecules (calcd 24.3% for **I** and 23.3% for **II**), and the final mass loss of 4% in the region 300–350 °C corresponds to the loss of the OH group (calcd 3.9% for **I** and 3.88% for **II**). In **III** and **IV**, the mass loss occurs in two steps with the second step having a large tail. For **III**, the mass loss of 9.8% occurring at 170 °C corresponds to the loss of free water (calcd 10.2%), and the second total mass loss including the tail of 33.3% occurring in the temperature range 250–550 °C corresponds to the loss of oxalate and amine (calcd 31%). In the case of **IV**, the mass loss of 8.7% occurring at 140 °C corresponds to the loss of free water (calcd 10.1%), and the second mass loss including the tail of 34.4% in the temperature range 300–600 °C corresponds to the loss of oxalate and the amine (calcd 32.1%). In all the cases, the final decomposed products were poorly crystalline and showed broad X-ray diffraction lines that correspond to the condensed iron phosphate $FePO_4$ [JCPDS: 29-0715].

Conclusion

Four new iron phosphate – oxalates belonging to the hybrid inorganic – organic family of open-framework structures have been synthesized hydrothermally in the presence of structure-

directing amines. Compounds **III** and **IV** are formed with the amine molecules within the framework, but **I** and **II** are devoid of the amines. All the compounds have the oxalate unit acting as the bridge between the layers. The layers in **I** and **II** are purely inorganic (formed only FeO_6 and PO_4 units), whereas **III** and **IV** have hybrid layers containing oxalate units in addition to FeO_6 and PO_4 moieties. Such a dual role of the oxalate unit is noteworthy. The formation of two types of inorganic layers in **I** and **II** suggest that the interconversions between the various sizes are facilitated by small energy changes. The observation of antiferromagnetic interactions in all the compounds shows that superexchange is facilitated through the phosphate and oxalate moieties. It would be worthwhile exploring the possibility of introducing other magnetic elements such as cobalt, and manganese as part of the iron phosphate–oxalate framework, to obtain materials with novel magnetic properties. Work on this theme is currently in progress and our initial results indicate that one can indeed form such hetero-substituted frameworks.

Experimental Section

Synthesis and initial characterization: The iron oxalate–phosphates **I**–**IV** were prepared under mild hydro/solvothermal conditions starting from a mixture of $FeCl_3$, H_3PO_4, and oxalic acid with an organic amine. The synthetic conditions are presented in Table 6. The starting mixtures were stirred to attain homogeneity and then sealed in 30 mL polypropylene bottles. All the chemicals were purchased from Aldrich and were used without any further purification. The initial pH of the mixture was 2.0 and the fill-factor was ≈40%. The mixtures after the heat treatments did not show any appreciable change in the pH (2.0). The reaction led to the formation of large quantities of transparent colorless rodlike (**I**), pale pink octahedral (**II**), and platelike (**III** and **IV**) crystals. The yields of the products were 20 (**I**), 60 (**II**), 50 (**III**), and 45% (**IV**), respectively. These crystals were used for all further studies. Initial characterization was carried out by subjecting the materials to powder X-ray diffraction (XRD), as well as to different forms of analysis, including thermogravimetric analysis (TGA), energy dispersive X-ray analysis (EDAX), and IR spectroscopy. XRD patterns on the powdered crystals indicated that the products were new; the patterns were entirely consistent with the structures determined by single-crystal X-ray diffraction. TGA studies revealed the content of water and oxalate in **I** and **II** and that of the oxalate and amine in **III** and **IV**. EDAX analysis gave the metal:phosphorus ratios. Infrared spectra showed

Table 6. Synthesis conditions and analysis for compounds **I**–**IV**.

Synthetic conditions			Analysis			Composition
			EDAX	TGA		
Mole ratio	Temp [°C]	Time [h]	Fe/P	Free H_2O [%]	Bound H_2O, oxalate + amine [%]	
$FeCl_3$:2 H_3PO_4:$H_2C_2O_4\cdot 2H_2O$:CHA:122 H_2O	110	120	1:1	4	27	$[Fe_2(H_2O)_2(HPO_4)_2(C_2O_4)]\cdot H_2O$ (**I**)
$FeCl_3$:2 H_3PO_4:$H_2C_2O_4\cdot 2H_2O$:CHA:122 H_2O	110	220	1:1	8.3	27	$[Fe_2(H_2O)_2(HPO_4)_2(C_2O_4)]\cdot H_2O$ (**II**)
$FeCl_3$:6 H_3PO_4:$H_2C_2O_4\cdot 2H_2O$:21,3-DAP:200 H_2O	110	96	1:1	9.8	33.3	$[C_3N_2H_{12}][Fe_2(HPO_4)_2(C_2O_4)_{1.5}]_2$(**III**)
$FeCl_3$:2 H_3PO_4:$H_2C_2O_4\cdot 2H_2O$:1,3-DAHP:200 H_2O	110	144	1:1	8.7	34.4	$[C_3N_2OH_{12}][Fe_2(HPO_4)_2(C_2O_4)_{1.5}]_2$ (**IV**)

Table 7. Crystal data and structure refinement parameters for compounds **I**–**IV**.

	I	**II**	**III**	**IV**
empirical formula	$Fe_2P_2O_{15}C_2H_8$	$Fe_2P_2O_{16}C_2H_{10}$	$Fe_4P_4O_{34}C_9N_2H_{28}$	$Fe_4P_4O_{35}C_9N_2H_{28}$
crystal system	monoclinic	monoclinic	monoclinic	monoclinic
space group	$P2_1/c$	$P2_1/c$	$P2_1/n$	$P2_1/n$
crystal size [mm]	0.08 × 0.1 × 0.16	0.08 × 0.12 × 0.16	0.08 × 0.12 × 0.16	0.08 × 0.12 × 0.16
a [Å]	4.840(2)	7.211(1)	9.214(1)	9.266(1)
b [Å]	17.571(6)	9.294(1)	15.201(2)	15.204(1)
c [Å]	7.342(4)	9.567(1)	12.046(1)	11.984(1)
β [°]	106.6(1)	103.4(1)	101.9(1)	102.2(1)
volume [Å^3]	598.5(4)	623.8(1)	1650.9(3)	1650.5(2)
Z	4	4	4	4
formula mass	445.7	463.7	527.7	535.7
ρ_{calcd} [g cm^{-3}]	1.930	1.852	2.152	2.152
λ ($Mo_{K\alpha}$) [Å]	0.71073	0.71073	0.71073	0.71073
μ [mm^{-1}]	2.093	2.008	2.045	2.044
θ range [°]	2.32–23.25	2.90–23.33	2.19–23.31	2.19–23.29
total data collected	2410	2532	6765	6801
index ranges	$-5\le h\le 5$, $-18\le k\le 19$, $-4\le l\le 8$	$-8\le h\le 7$, $-10\le k\le 6$, $-10\le l\le 10$	$-10\le h\le 10$, $-16\le k\le 13$, $-11\le l\le 13$	$-10\le h\le 9$, $-16\le k\le 16$, $-7\le l\le 13$
unique data	857	894	2387	2370
observed data ($\sigma > 2\sigma(I)$)	781	747	1533	1617
refinement method	full-matrix least-squares on $\lvert F^2\rvert$	full-matrix least-squares on $\lvert F^2\rvert$	full-matrix least-squares on $\lvert F^2\rvert$	full-matrix least-squares on $\lvert F^2\rvert$
R_{merg}	0.04	0.03	0.08	0.08
R indexes [$I > 2\sigma(I)$]	$R = 0.03$,[a] $wR_2 = 0.06$[b]	$R = 0.03$, $wR_2 = 0.08$	$R = 0.06$, $wR_2 = 0.14$	$R = 0.08$, $wR_2 = 0.18$
goodness of fit (S)	1.11	1.13	1.04	1.14
no. of variables	118	117	232	236
largest difference map peak and hole [e Å^{-3}]	0.455/−0.402	0.360/−0.422	1.408/−0.711	1.547/−0.734

[a] $R_1 = \Sigma\,||F_o| - |F_c||/\Sigma\,|F_o|$. [b] $wR_2 = \{\Sigma[w(F_o^2 - F_c^2)^2]/\Sigma[w(F_o^2)^2]\}^{1/2}$, $w = 1/[\sigma^2(F_o)^2 + (aP)^2 + bP]$, $P = [\max.(F_o^2,0) + 2(F_c)^2]/3$, where $a = 0.0239$ and $b = 1.1632$ for **I**, $a = 0.049$ and $b = 0.0$ for **II**, $a = 0.9$ and $b = 0.0$ for **III** and $a = 0.0423$ and $b = 33.461$ for **IV**.

0947-6539/00/0607-1174 $ 17.50+.50/0 *Chem. Eur. J.* **2000**, *6*, No. 7

the absence of the amine in **I** and **II**. The results of the analysis on the synthesized products are presented in Table 6. The composition of the various iron phosphate – oxalates were calculated to be as follows: **I**, $Fe_2(H_2O)_2(HPO_4)_2(C_2O_4)\cdot H_2O$, **II**, $Fe_2(H_2O)_2(HPO_4)_2(C_2O_4)\cdot 2H_2O$, **III**, $[C_3N_2H_{12}][(Fe_2(HPO_4)_2(C_2O_4)_{1.5}]_2$, and **IV**, $[C_3N_2OH_{12}][(Fe_2(HPO_4)_2(C_2O_4)_{1.5}]_2$. These compositions exactly agree with those derived from X-ray crystallography. Compositionally **I** and **II** are similar except for the water of hydration. Structures of **III** and **IV** differ with respect to the composition of the amine. Magnetic susceptibility measurements on all the four compounds were carried out in the 30 – 300 K range using a Lewis coil magnetometer.

Single-crystal structure determination: A suitable single crystal of each compound was selected carefully under a polarizing microscope and mounted at the tip of a glass fiber using cyanoacrylate (superglue) adhesive. Crystal structure determination by X-ray diffraction was performed on a Siemens Smart-CCD diffractometer equipped with a normal focus, 2.4 kW sealed tube X-ray source ($Mo_{K\alpha}$ radiation, $\lambda = 0.71073$ Å) operating at 50 kV and 40 mA. A hemisphere of intensity data were collected at room temperature in 1321 frames with ω scans (width of 0.30° and exposure time of 20 s per frame). The final unit cell constants were determined by a least-squares fit of 1822 reflections for **I**, 1681 reflections for **II**, 2562 reflections for **III**, and 2549 reflections for **IV** in the range $4 \leq 2\theta \leq 46.5$ and are presented in Table 7.

The structure was solved by direct methods using SHELXS-86[16] and difference Fourier syntheses. For compounds **I** and **II**, the hydrogen positions were easily located in the difference Fourier maps and for the final refinement the hydrogen atom on one of the oxygen atoms [O(7)] was placed geometrically and held in the riding mode. In the case of **III** and **IV**, both the amine and water molecules were disordered, and the location of the hydrogen positions for these molecules was not possible. The hydrogen atoms on the oxygen atoms [O(13), O(14)] were, however, located in the difference Fourier maps and were placed geometrically and held in the riding mode. The disorder of the amine molecules in **III** and **IV** made it difficult to refine anisotropically. The last cycles of refinement included atomic positions, anisotropic thermal parameters for all the non-hydrogen framework atoms, and isotropic thermal parameters for all the hydrogen atoms. Full-matrix least-squares structure refinement against $|F^2|$ was carried out using the SHELXTL-PLUS[17] package of programs. Pertinent refinement parameters are presented in Table 6. Further details of crystal structure investigations may be obtained from the Fachinformationszentrum, Karlsruhe, D-76344, Eggenstein-Leopoldshagen, Germany (fax: (+49) 7247-808-666; e-mail: crysdata@fiz-karlsruhe.de) on quoting the depository numbers CSD-391074 (**I**), CSD-391075 (**II**), CSD-391076 (**III**), and CSD-391077 (**IV**).

[1] *Atlas of Zeolite Structure Types* (Eds.: W. H. Meier, D. H. Olson), Butterworth-Heinemann, London, **1992**; *Handbook of Heterogeneous Catalysis* (Eds.: G. Ertl, H. Knözinger, J. Weitkamp), VCH, Berlin **1997**; A. K. Cheetham, G. Ferey, T. Loiseau, *Angew. Chem.* **1999**, *111*, 3466; *Angew. Chem. Int. Ed.* **1999**, *38*, 3268.

[2] S. Natarajan, *J. Solid State Chem*. **1998**, *139*, 200.

[3] P. Lightfoot, Z. A. D. Lethbridge, R. E. Morris, D. S. Wragg, P. A. Wright, Å. Kvick, G. B. M. Vaughan, *J. Solid State Chem*. **1999**, *143*, 74.

[4] Y.-F. Huang, K.-H. Lii, *J. Chem. Soc. Dalton Trans.* **1998**, 4085; H.-M. Lin, K.-H. Lii, Y.-C. Jiang, S.-L. Wang, *Chem. Mater*. **1999**, *11*, 519.

[5] Z. A. D. Lethbridge, P. Lightfoot, *J. Solid State Chem*. **1999**, *143*, 58.

[6] A. Choudhury, S. Natarajan, C. N. R. Rao, *J. Solid State Chem*. **1999**, *146*, 538.

[7] A. Choudhury, S. Natarajan, C. N. R. Rao, *Chem. Mater*. **1999**, *11*, 2316.

[8] I. D. Brown, D. Altermatt, *Acta Crystallogr. B* **1985**, *41*, 244.

[9] M. Cavellec, D. Riou, C. Ninclaus, J.-M. Gerenèche G. Férey, *Zeolites* **1996**, *17*, 250; K.-H. Lii, Y.-F. Huang, V. Zima, C.-Y. Huang, H.-M. Lin, Y.-C. Jiang, F.-L. Liao S.-L. Wang, *Chem. Mater*. **1998**, *10*, 2599.

[10] W. T. A. Harrison, L. L. Dussack, A. J. Jacobson, *J. Solid State Chem*. **1996**, *125*, 234.

[11] S. Natarajan, J.-C. P. Gabriel, A. K. Cheetham, *Chem. Commun*. **1996**, 1415, and references therein.

[12] X. Bu, P. Feng, T. E. Gier, G. D. Stucky, *J. Solid State Chem*. **1998**, *136*, 210.

[13] S. Ayyappan, X. Bu, A. K. Cheetham, S. Natarajan, C. N. R. Rao, *Chem. Commun*. **1998**, 2181.

[14] R. Vaidhyanathan, S. Natarajan, A. K. Cheetham, C. N. R. Rao, *Chem. Mater*. **1999**, *11*, 3636.

[15] C. Mathoniere, S. G. Carling, P. Day, *J. Chem. Soc. Chem. Commun*. **1994**, 1551, and references therein.

[16] G. M. Sheldrick, SHELXS-86 Program for Crystal Structure Determination, University of Göttingen **1986**; G. M. Sheldrick, *Acta Crystallogr*. **1990**, *A35*, 467.

[17] G. M. Sheldrick, SHELXTL-PLUS Program for Crystal Structure Solution and Refinement, University of Göttingen, **1993**.

Received: August 23, 1999 [F1993]